Generative Multi-Functional Meta-Atom and Metasurface Design Networks

Sensong An[1], Bowen Zheng[1], Hong Tang[1], Mikhail Y. Shalaginov[2], Li Zhou[1], Hang Li[1], Tian Gu[2], Juejun Hu[2], Clayton Fowler[1,*], Hualiang Zhang[1,*]

[1]Department of Electrical & Computer Engineering, University of Massachusetts Lowell, Lowell, MA 01854, USA
[2]Department of Materials Science & Engineering, Massachusetts Institute of Technology, Cambridge, MA 02319, USA
**e-mail address: clayton_fowler@uml.edu, hualiang_zhang@uml.edu*

Abstract

Metasurfaces are being widely investigated and adopted for their promising performances in manipulating optical wavefronts and their potential for integrating multi-functionalities into one flat optical device. A key challenge in metasurface design is the non-intuitive design process that produces models and patterns from specific design requirements (commonly electromagnetic responses). A complete exploration of all design spaces can produce optimal designs but is unrealistic considering the massive amount of computation power required to explore large parameter spaces. Meanwhile, machine learning techniques, especially generative adversarial networks, have proven to be an effective solution to non-intuitive design tasks. In this paper, we present a novel conditional generative network that can generate meta-atom/metasurface designs based on different performance requirements. Compared to conventional trial-and-error or iterative optimization design methods, this new methodology is capable of producing on-demand freeform designs on a one-time calculation basis. More importantly, an increased complexity of design goals doesn't introduce further complexity into the network structure or the training process, which makes this approach suitable for multi-functional device designs. Compared to previous deep learning-based metasurface approaches, our network structure is extremely robust to train and converge, and is readily expanded to many multi-functional metasurface devices, including metasurface filters, lenses and holograms.

Keywords: multi-functional, metasurface, meta-atom, generative adversarial network, conditional GAN, Wasserstein GAN, deep learning, neural networks, inverse design

Introduction

Metasurfaces, the two dimensional (2D) versions of metamaterials, are planar/conformal devices composed of subwavelength structures, called meta-atoms [1, 2], that are able to tailor both the amplitude and phase of incident waves [3-5]. By manipulating the geometry of the individual meta-atoms to excite electromagnetic (EM) multipoles within, independent phase and amplitude control can be achieved at the element level. Recently, metasurfaces consisting of all-dielectric meta-atoms have drawn enormous attention [4, 6-8], due to their unique capability of supporting

magnetic multipole resonances and their superior efficiency at optical and infrared wavelengths as compared to their metallic counterparts [9-12]. The multipole responses in a meta-atom can be highly complicated even for simple shapes, and thus a meta-atom's EM response to an incident EM wave is difficult to predict. As such, it can be time-consuming and laborious to find an appropriate set of meta-atoms for a design. Traditional design approaches largely rely on iterative numerical full-wave simulations (e.g. finite-element method (FEM), finite-difference time-domain (FDTD) method and finite integration technique (FIT)), which provide accurate device response predictions, but are severely time consuming. Moreover, the design process relies on empirical reasoning or trial-and-error [4, 7], which is inefficient and often ineffective, especially with highly nonlinear problems, such as multifunctional metasurface/meta-atom designs.

To solve non-intuitive meta-atom/metasurface design challenges, several deep neural network (DNN) based approaches were proposed and investigated beginning in 2018. One widely-employed approach [13-18] requires a pre-trained simulator for fast electromagnetic performance evaluations, which was later combined with another model generator to build a "tandem" inverse design neural network. This "tandem network" structure overcomes the non-uniqueness of solutions existing in all inverse design problems, allowing the inverse neural network to converge and generate a unique solution for each single requirement. However, there are several limitations with this approach. Firstly, the performance of the generator is very much limited by the pre-trained simulator, hence the scope of input training datasets. Once the generator comes up with a design solution that exceeds the outer boundary of the training datasets, it would be automatically disqualified since the simulator would be unable to predict its performance correctly. As a result, the training datasets must be chosen carefully to ensure their variety and coverage. This can quickly become computationally laborious, considering that the parameter space increases exponentially for each parameter introduced. Secondly, the "tandem" inverse design networks can only generate one single design based on each input specification, which suggests they are "memorizing the solution" rather than "learning and composing". Lastly, designs from all these works are based on variations of simple canonical geometries that can be easily defined by several parameters, such as bulk layers, metallic rings, dielectric spheres and cylinders, etc. Training of these tandem networks can be extremely difficult for metasurfaces with freeform geometries because of the huge mismatch between required EM response inputs and large design parameter outputs.

Generative Adversarial Networks (GAN) provides a possibility to mitigate these challenges. Since the concept of GAN was firstly introduced in 2014 [19], it has been widely studied and applied in the field of image processing due to its unique ability to compose complex and diverse designs based on limited inputs once the hidden distributions behind the enormous amount of training datasets were revealed and learned. Within GANs, a generator network learns to map from a latent space to a specified data distribution, while the discriminator network tries to distinguish the candidates given by the generator from those pulled from the real data distribution. Repeated comparisons between generated and real data continually improve the performance of both the generator and the discriminator until the generated data becomes indistinguishable from the real data. The adversarial nature between the generator and discriminator also explained why the training process is difficult with a pre-trained discriminator that is adopted in "tandem" networks: the well-trained discriminator can always distinguish the real and fake samples, which caused the back propagated generator gradient hard to descend.

The Conditional Generative Adversarial Nets (CGAN) [20], a variant of the original GAN that is able to generate required designs conditioned on class labels, was recently introduced into metasurface designs for realization of metallic metasurface modulators with defined transmission spectrum [14] and meta-gratings with specified beam deflection angles and working frequencies [21-23]. However, these existing GAN-enabled metasurface design networks are either dealing exclusively with amplitude responses [14] or dealing with meta-grating designs at a supercell level [21-24]. Due to the unpredictable phase jumps that are introduced by electromagnetic poles [22], a GAN-enabled meta-atom design approach that deals with both amplitude and phase responses is more challenging and has been an open question. This significantly limited the efficacy of DNN-based metasurface design approaches, since most of metasurface devices for high-frequency applications, such as beam deflectors, lenses, polarizers and holograms, rely on reshaping the phase front of electromagnetic waves.

Design of multifunctional metasurfaces, e.g. phase-change reconfigurable metasurfaces, multi-wavelength metasurfaces [9, 10, 25, 26] and multi-polarization metasurfaces [27], has remained challenging due to the large number of degrees of freedom needed to satisfy design goals under different conditions. Traditional design approaches largely rely on trial-and-error [9, 10] or evolutional algorithms [25, 27] to search for meta-atoms with basic shapes, such as rings [9, 10], cubes [26, 28] or cylinders [29], to meet design criteria. These approaches limit the design degrees of freedom and often require full-wave simulation verifications, and are thus time-consuming. In contrast, inverse design methods employing GAN-enabled networks reduced design restrictions by enabling freeform patterns that are generated on a one-time calculation basis once the training is done. Moreover, neural networks handles multiple inputs in parallel, meaning the design complexity of deep-learning-enabled metasurface inverse design networks (constructed either with fully-connected layers or convolutional layers) is not affected by the size of the inputs. This again strengthens GAN's potential in tackling multifunctional inverse design problems.

In this work, we present a novel approach for designing freeform all-dielectric meta-devices combining the CGAN with the Wasserstein Generative Adversarial Networks (WGAN) [30, 31] structure. As another widely-adopted GAN variant, WGAN introduced Earth-Mover distance as loss evaluation method, which not only stabilized the training process, but also made the network compatible to universal regression problems, including on-demand meta-atom designs. This conditional Wasserstein GAN we constructed tackles both phase-related meta-atom design and multi-functional metasurface design challenges. For the first time, a GAN-based deep-learning framework for multifunctional meta-atom/metasurface designs has been demonstrated. Specifically, we present a new form of the Gradient Penalty (GP) method, together with a split complex coefficient data feeding approach for the custom optimization of meta-atom design problems. The proposed network has a resilient architecture, can easily stabilize and converge during training, and be readily extended to a variety of multifunctional metasurface designs. Based on this highly efficient meta-atom design network, several metasurface devices including a hologram, a filter and a reconfigurable metalens were designed and verified to illustrate the versatility and scalability of the method. The design examples employing this network structure substantiate that the proposed approach accomplished the following important goals: 1. the first

freeform all-dielectric meta-atom design network, 2. the first freeform multifunctional metasurface design network and 3. the first metasurface-based lens and hologram designed by GANs.

Method

Network architecture. The proposed network (Fig. 1 a, b) combines the WGAN structure with the method of a conditional-GAN, which learns the mapping method from the conditions x and random latent vector z, to a target design y', defined as: $y' = G(z|x)$. Since metasurfaces are two-dimensional (2D) versions of metamaterials, here we fixed the height of each meta-atom and treated them as 2D images. The spectral phase and amplitude responses found from numerical simulation of real samples y are used as the conditions for the proposed network, and are combined with a 1 × 100 latent vector z that obeys a Gaussian distribution (Fig. 1a). This joint input was fed into the constructed generator to yield fake samples y'. The following discriminator calculates the Wasserstein distance between the real samples y and the generated fake ones $y'$and inversely tunes the parameters within the generator/discriminator to minimize/maximize the Wasserstein distance through gradient descent algorithms:

$$W(P_{data}, P_G) \approx \max_D \{E_{y\sim P_{data}}[D(y|x)] - E_{y'\sim P_G}[D(y'|x)]\} \quad (1)$$

The parameter optimizations for the generator and the discriminator are processed in turns, aiming for opposite objectives: the generator G is trained to produce samples that cannot be distinguished by the discriminator, while the discriminator is trained to detect generated samples as fake. After the model is fully trained, the loss of both the generator and the discriminator, defined as:

$$L_g = -E_{y'\sim P_G}[D(y'|x)] \quad (2)$$

$$L_d = E_{y'\sim P_G}[D(y'|x)] - E_{y\sim P_{data}}[D(y|x)] \quad (3)$$

should be minimized and stabilized. Once both generator and discriminator are constructed with enough capacity, their stabilized loss indicates that they have reached a point at which both cannot be improved because P_g already equals P_{data}. At this point, the generator can generate samples close enough to the real samples that the discriminator is unable to differentiate between the real sample distribution and the fake sample distribution.

Detailed network structures of the discriminator and generator are shown in Fig. 1b. We used Leaky ReLu-BatchNorm-transposed convolution modules [32, 33] for the generator, and ReLu-BatchNorm-convolution modules for the discriminator. All meta-atom patterns collected to form the training datasets were rescaled into 64 x 64 pixel images before they were fed into the discriminator for evaluation. Depth of each 64 x 64 image is gradually increased while their 2D dimensions are decreased when passed through (2, 2) stride convolutional layers. The output of each layer is batch-normalized and passed through a ReLU activation function before it is passed on to the next layer. The generator takes the conditioned distribution $(z|x)$ as input, which is then provided to seven consecutive transposed convolutional layers. Each layer is followed by a leaky ReLU activation function for conditioned image generation. After the last transposed convolutional layer, a tanh activation function generates an image ready for evaluation.

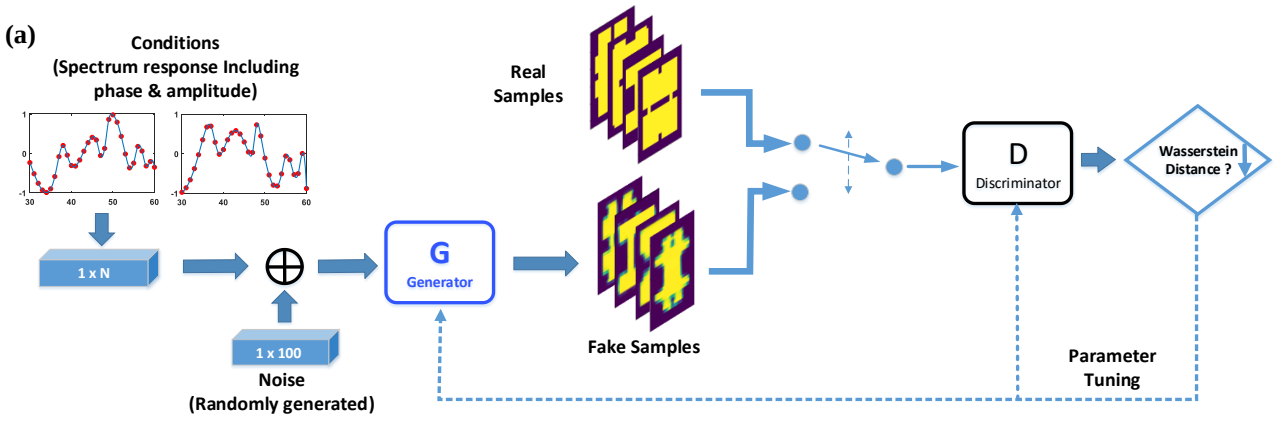

(b)

Layer	Output tensors
1	64×64×32
2	64×64×32
3	32×32×32
4	16×16×64
5	8×8×128
6	4×4×256
7	2×2×512
8	1

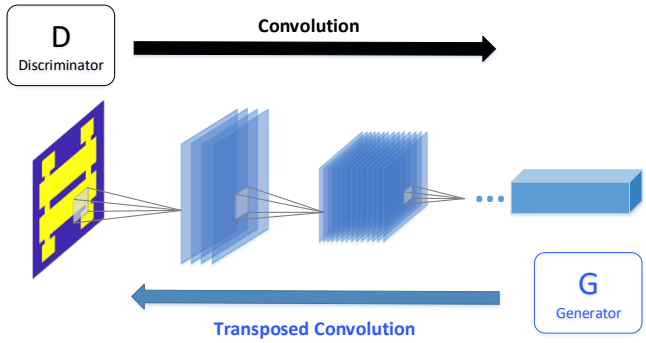

Layer	Output tensors
1	4x4x512
2	8x8x256
3	16x16x128
4	32x32x64
5	64x64x32
6	64x64x32
7	64x64x32
8	64x64x1

Figure 1. Network architecture of the generative meta-atom design network. (a) Schematic diagram of the proposed network. The discriminator network measures the Wasserstein distance between inputs and aims to maximize the distance between real and fake samples. The generator network transforms target conditions combined with noise prior to producing fake samples that resemble real ones well enough to confuse the discriminator. Both components approach the real data distribution through parameter tuning during this adversarial process. **(b)** Detailed structure of the generator and discriminator. Shapes of output tensors for each layer in these two components are listed in the blue and black tables, respectively.

Training data collection. The all-dielectric meta-atom under consideration consists of a 1 μm thick dielectric component (preferably with a high refractive index) placed on a dielectric substrate (preferably with a lower refractive index) with a unit cell size of 2.8 x 2.8 μm^2, which is designed to operate in the 5-10 μm spectrum range (Fig. 2a). Without loss of generality, each meta-atom was generated with the "Needle Drop" approach using numerical computing tool MATLAB. Several (3 to 7) rectangular bars, with a minimum generative resolution of 0.1 μm, were randomly generated and placed together within a square lattice to form random patterns (Fig. 2b). To minimize inter-cell coupling, a minimum spacing of 0.4 μm was applied between adjacent meta-atoms. To speed up the data-collection process, the all-dielectric components are only generated in the top left quadrant of each lattice and then symmetrically replicated along x and y axes to form the whole pattern.

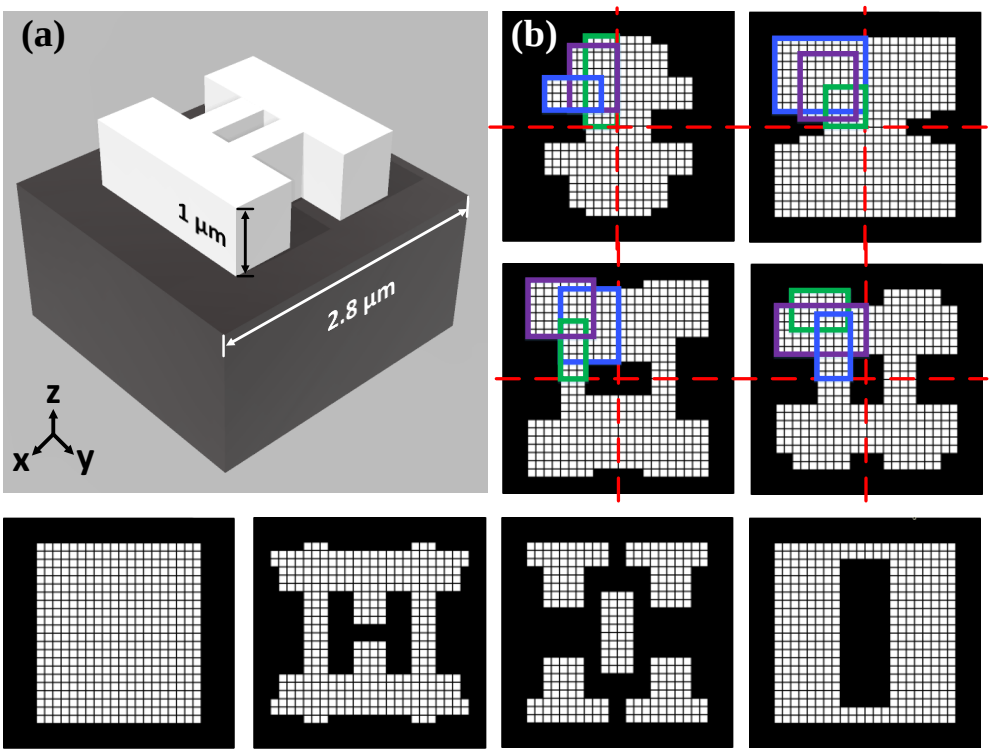

Figure 2. Training data collection process. (a) View of a randomly generated meta-atom. Lattice size for each meta-atom cell is 2.8 μm, while the height of the high-index dielectric structures is fixed to be 1 μm. White represents high-index dielectric components, while black represents the low-index substrate. **(b)** Demonstration of the pattern generation process. 2D patterns in x-y plane are meshed for better view, each mesh has a dimension of 0.1 by 0.1 μm^2. Rectangles outlined in different colors represent distinct high-index "Needles" that were randomly generated and dropped on the top-left quadrant of the substrate canvas. Patterns were completed by mirroring along the x and y axes.

The full-wave electromagnetic simulations were performed using the commercial software package CST Microwave Studio Suite. For each meta-atom, perfect electric conducting surface ($E_t = 0$) and perfect magnetic conducting surface ($H_t = 0$) boundary conditions were employed to calculate the transmission and phase shift of a square lattice structure. Open boundaries are applied along both the negative and positive z directions, while an x-polarized plane wave was illuminated from the substrate side for each meta-atom. To further accelerate the full-wave simulations, $E_t = 0$ and $H_t = 0$ symmetry planes were applied in the center y-z plane and x-z plane for each meta-atom, respectively. A total number of 69,000 meta-atoms with different shapes were generated and simulated to find their wide-spectrum phase and amplitude responses. After removing similar patterns, 29,000 patterns were selected and documented for further training.

Customized gradient-penalty method. From equation (1) we can conclude that the Wasserstein distance is only accurate when the discriminator is a 1-Lipschitz function [30]. To enforce this constraint, the original WGAN applied a simple, but rough, value clipping to restrict the maximum weight value in each layer of the discriminator. Instead, the WGAN-GP uses a gradient penalty term to ensure that the norm of its gradients is equal to 1 almost everywhere [31] so that the discriminator is 1-Lipschitz. The WGAN with gradient penalty term can be represented as:

$$W(P_{data}, P_G) \approx \sup_{\|D\|_L \leq 1} \Big\{ E_{y \sim P_{data}}[D(y|x)] - E_{y' \sim P_G}[D(y'|x)] - \lambda E_{x \sim P_{penalty}}[\max(0, \|\nabla_x(D(x))\| - 1)] \Big\} \quad (4)$$

The traditional WGAN-GP randomly interpolates between network generated patterns $P_{generator}$ and real sample patterns P_{data} to generate gradient penalty samples $P_{penalty}$, as shown in Fig. 3a. The major advantage of this interpolation method is as follows: as the training progresses and $P_{generator}$ approaches P_{data}, the gradient norm of this more widespread distribution $P_{penalty}$, instead of the real sample distribution P_{data}, satisfies the Lipschitz constraint, and we can thus conclude that the discriminator is 1-Lipschitz almost everywhere within P_{data}.

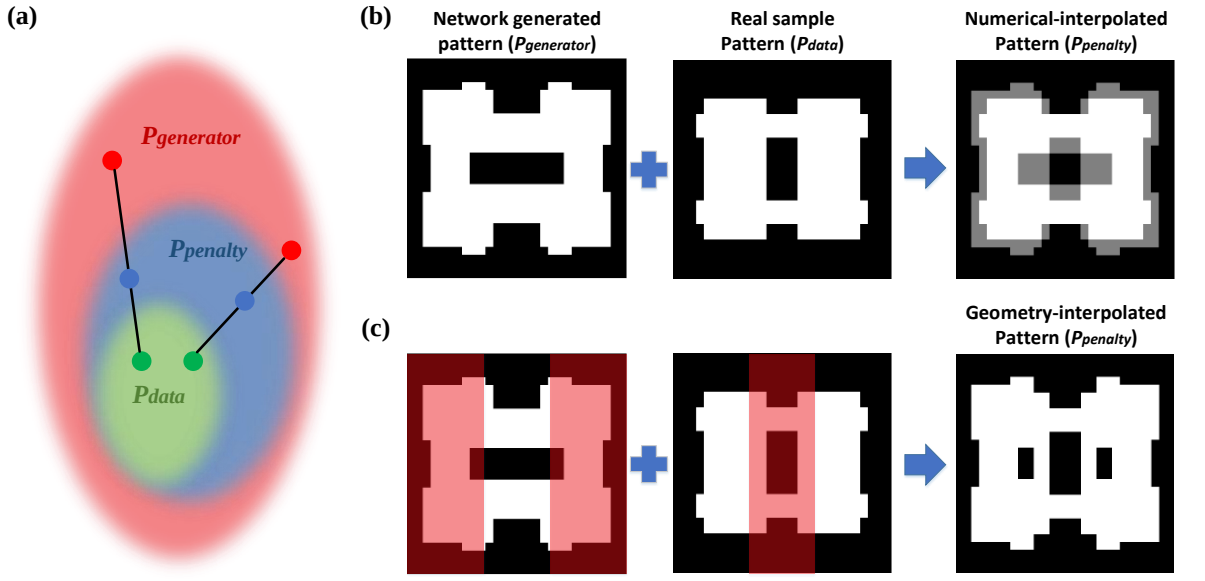

Figure 3. A novel interpolation method for customized gradient penalty. (a) Schematic diagram of the random interpolation process in WGAN-GP. The network randomly interpolates between $P_{generator}$ and P_{data} to get $P_{penalty}$. **(b)** Numerical interpolation methods employed by traditional WGAN-GPs. The meta-atom patterns are binarized, such that white represents "1" and black represents "0". (c) The proposed novel geometry interpolation method. Random proportions (marked in red) were taken from both fake samples and real samples and later combined into a new pattern.

In our case, with meta-atom patterns as targeted design goals, the generated outputs can be converted into binary images consisting of 1's that represent the existence of dielectric materials and 0's that represent voids. Fig. 3b demonstrates how the conventional numerical interpolation process won't work well for the meta-atom discriminator. Values between "0" and "1" are generated which don't correspond to any types of physical structures. During the training process, discriminator that is trained to satisfy the Lipschitz constraint for this $P_{penalty}$ is intuitively hard to yield stable Wasserstein distance results for real samples from P_{data}. Instead, we employed a novel geometry interpolation method that takes random geometry proportions from both $P_{generator}$ and P_{data}. Different counterparts were later combined together to form the sample in $P_{penalty}$ (Fig. 3c), which fully characterizes the sample between the $P_{generator}$ and P_{data}. Later training experiments verified the training stability and design accuracy of this method.

Results and Discussion

Conditions of the proposed generative network structure are formed with single or multiple related/unrelated design specifications, which means this network has the unique ability to deal with multifunctional meta-atom/metasurface designs. To fully explore its potential, in the following we discuss the construction and training results of three individual networks including a single-frequency meta-atom design network and two multifunctional metasurface design networks. Based on these generative meta-atom design networks, design and verification of an all-dielectric hologram, a dual-polarized metalens with polarization-dependent focal lengths, a polarization-independent lens and several broadband metasurface modulators are presented.

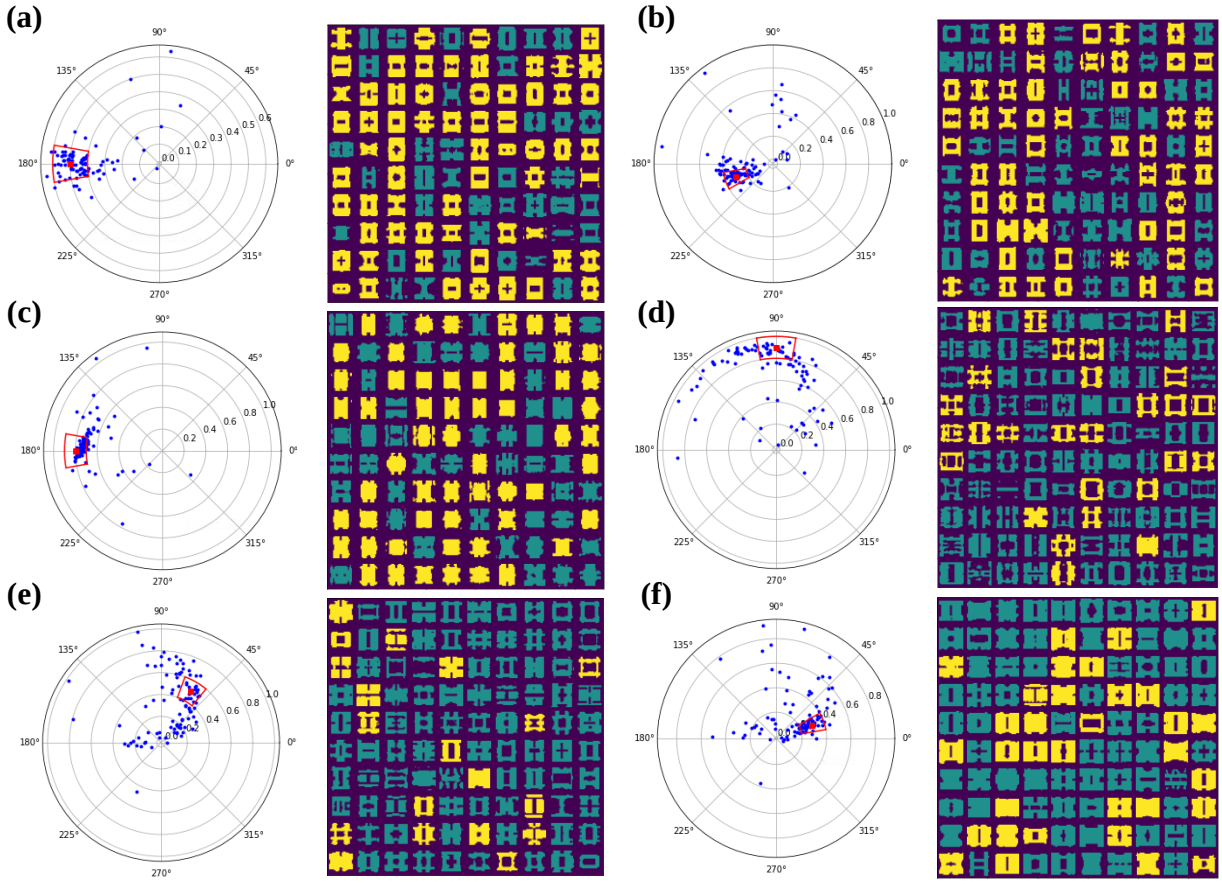

Figure 4. Meta-atom designs generated using a fully-trained conditional WGAN model. 100 meta-atom designs are generated using the well-trained meta-atom design network for each combined amplitude and phase conditions, which are **(a)** 0.5 + 180°, **(b)** 0.3 + 200°, **(c)** 0.8 + 180°, **(d)** 0.9 + 90°, **(e)** 0.5 + 60° and **(f)** 0.3 + 20°, respectively. Blue dots represent EM responses of generated designs, red dots represent the targeted amplitude and phase conditions. A 2D pattern of each design is combined and shown on the right in each subplot. Red outlines in each polar plot indicate qualified designs, while the corresponding patterns are highlighted in yellow.

Meta-atom design network. A meta-atom design network was designed to generate meta-atom patterns based on conditioned phase and amplitude profiles following the proposed network architecture. Due to the phase-related design difficulties as mentioned in [18], a preprocessing layer that translates relative phase (with the all-void meta-atom set as zero phase) and amplitude

responses into complex transmission coefficients was added before the first layer of inputs. The real and imaginary parts of the transmission coefficients form the conditions x, such that $x = [T_{real}(y),\ T_{imag}(y)]$. Without loss of generality, the operating frequency was chosen to be 50 THz (6 μm). After 3,000 epochs of training, both the discriminator and generator losses were minimized and stabilized, indicating that the network is fully trained.

Several phase and amplitude combinations were chosen to test the trained network model. For each phase and amplitude combination, we employed the generator to consecutively run for 100 times to check the generation stability of the network. As shown in Fig. 4, targeted phase and amplitude combinations are marked with red dots, while the electromagnetic responses of generated patterns were simulated and labeled with blue dots. The pass rate for the trained model represents its ability to find the precise conditional distribution $P(y|x)$, and is a crucial performance indicator of the model. Since the generator will eventually generate a satisfactory design if given enough trials, a high pass rate is indicative of learning the right distribution rather than finding a design by chance. Here we adopted a minimum threshold of ±0.1 amplitude errors and ±10° phase errors, as outlined in red lines in each polar plot in Fig. 4. The number of qualified designs for each condition was counted and listed in Table 1. The low pass rates shown in (d) and (e) can possibly be improved by introducing ResNets, increasing the number of layers, and/or increasing the number of neurons per layer, which would all need future experimental testing.

Table 1. Design conditions used in Fig. 4 and corresponding pass rates

Figure	Amplitude (E-field)	Phase (degrees)	Qualified No. of Points	Pass rate
a	0.5	180	63	63%
b	0.3	200	52	52%
c	0.8	180	57	57%
d	0.9	90	27	27%
e	0.5	60	19	19%
f	0.3	20	34	34%

It is worth to mention that, by examining the meta-atom structures generated by the proposed network (as shown in Fig. 4), it may be possible to use a trained network to discover underlying physical characteristics behind a particular EM response. For example, almost all designs in Fig. 4f have a larger volume compared to the designs in Fig. 4a-e, while most qualified designs in Fig. 4d have a slim appearance with a large square hole in the middle. Qualified patterns in Fig. 4c can be roughly categorized into two categories: one has a similar rectangular shape (the upper half designs), while the other one looks like an “x” (several designs in the bottom half). By processing the image through several convolutional layers, the neural network discovered that these designs with different geometries have something in common and can be categorized into the same conditional distribution, which is non-intuitive and almost impossible for human brains. Moreover, training datasets collected with the “Needle Drop” approach are all composed of rectangles with straight sharp edges. While in Fig. 4a-f, designs with inclined edges and round corners are

generated, indicating the exploratory nature of the proposed network which resulted in output designs that broke away from training data limitations.

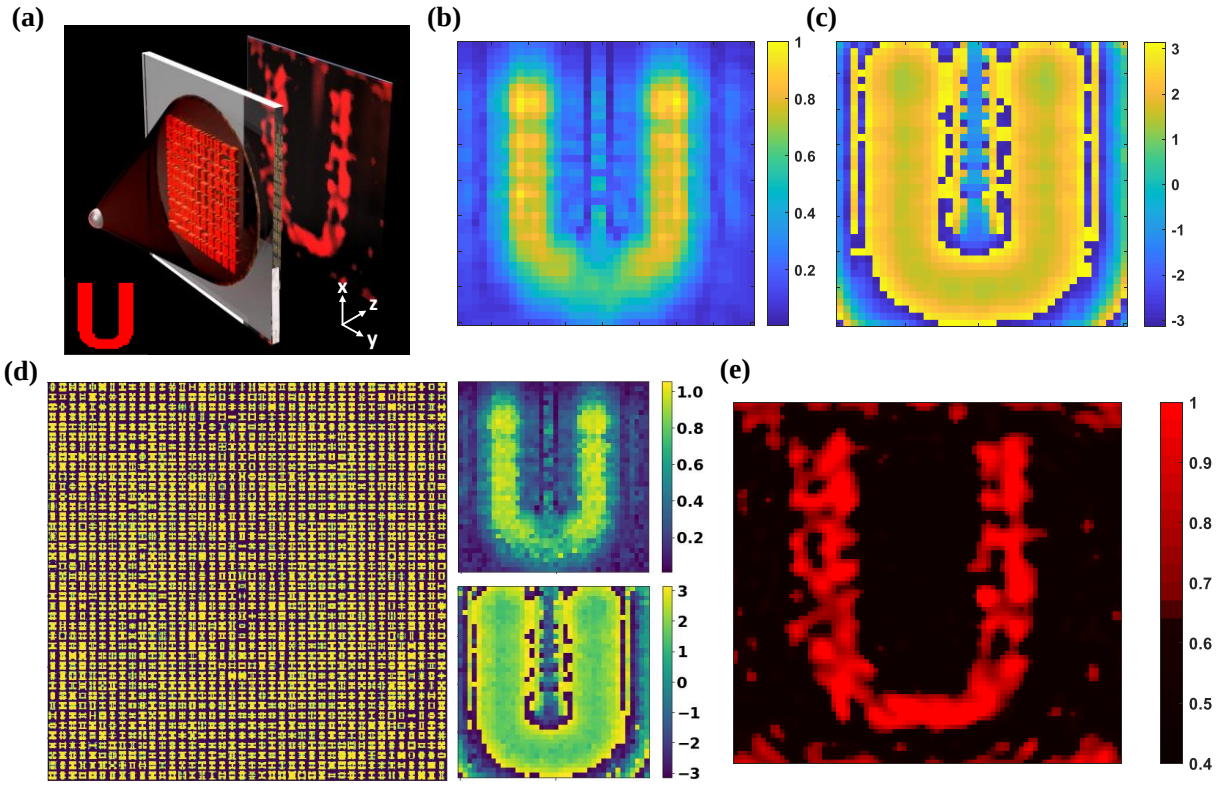

Figure 5. A hologram designed with the meta-atom generative network. (a) Front view demonstration of a flat metasurface hologram with the virtual object of a flat image "U". The metasurface is designed to be 112 by 112 μm^2, while the image plane is placed 56 μm away from the metasurface. **(b)** Targeted amplitude mask and **(c)** Targeted phase mask of the designed hologram. **(d)** Metasurface pattern designed by the meta-atom generative network, with its corresponding amplitude and phase masks shown as insets. **(e)** Full wave simulation results of the electric field on the image plane.

Using the trained network, we designed a transmissive metasurface hologram operating at 50 THz, which designates both amplitude and phase profiles of each meta-atom. For the convenience of full-wave simulation verification, the scale of this square-shaped hologram is designed to be relatively small (with 40x40 meta-atoms). The virtual object is assumed to be a flat screen with the image of a capitalized letter "U" (inset in Fig. 5a) that is placed 56 μm away from the metasurface. The corresponding amplitude and phase profiles required for each meta-atom were calculated according to the reversibility of beam propagation [3], and are shown in Fig. 5b and 5c, respectively. The final metasurface hologram design, along with the amplitude and phase profiles for each meta-atom as verified by CST, is shown in Fig. 5d. A full-wave simulation of the image reconstruction for the proposed metasurface hologram was also carried out (Fig. 5e). It is observed that full-wave simulation results agreed well with the designed image, which clearly validates the performance of the proposed network.

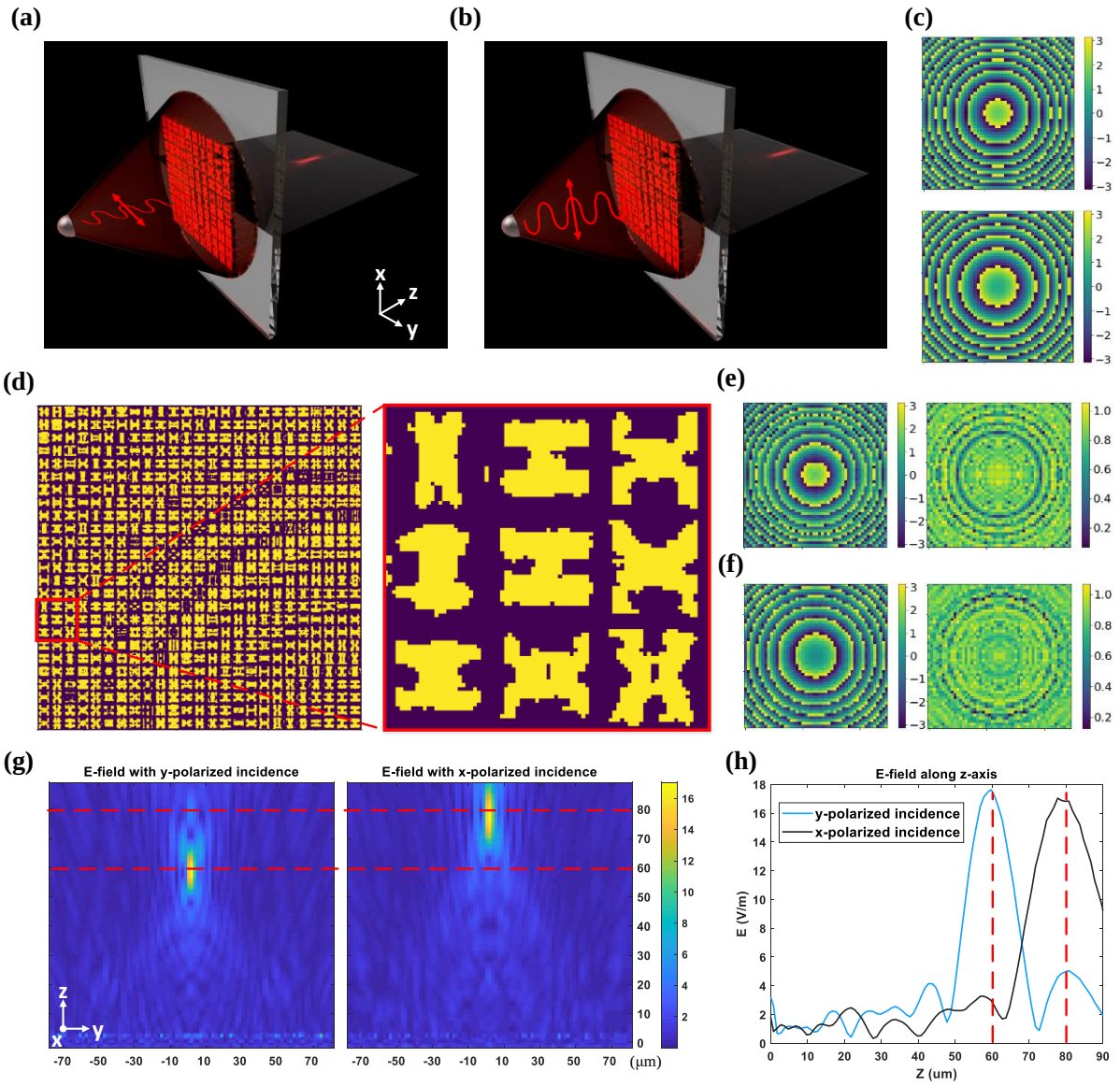

Figure 6. A focal-reconfigurable lens designed with the dual-polarization meta-atom generative network. (a) Front view demonstration of a focal-reconfigurable lens operating under y-axis linear polarization incidence and **(b)** x-axis linear polarization incidence. **(c)** Targeted phase masks for the focal-reconfigurable lens under x-polarization incidence and y-polarization incidence, respectively. **(d)** Metasurface pattern designed with the dual-polarization meta-atom generative network. Corresponding phase and amplitude masks under y and x polarized incidences are plotted in **(e)** and **(f)**, respectively. **(g)** Full wave simulated E-field in y-z plane under y and x-polarized incidence, respectively. The focal spot is clearly shifted from z = 60 μm to z = 80 μm when the polarization direction switched from y to x, which can also be seen in **(h)**, which shows the simulated E-field along optical axis under the two different incidences.

Multifunctional meta-atom design networks. The proposed network structure also deals with multi-functional meta-atom designs. For example, by simply enlarging and rearranging the condition vector: $x = [T_{real}(y),\ T_{imag}(y), T_{real}(y^T),\ T_{imag}(y^T)]$, the network is easily transformed into a polarization-reconfigurable meta-atom design network. After being fully-trained with data for the complex transmission coefficients collected under two orthogonal

polarization incident directions (along x and y-axis, respectively) at 55 THz, the generative model is able to generate meta-atom designs based on four distinct inputs: amplitude and phase responses for both x and y-polarized incidences. We demonstrate this technique with a network-generated transmissive focal-reconfigurable aspheric metalens working in the mid-IR range.

Fig. 6a, b present schematic diagrams of the working principles for the proposed focal-reconfigurable metasurface lens. The lens was designed to focus at 60 μm under y-polarized plane wave incidence and at 80 μm when illuminated with an x-polarized plane wave. The lens has a 140 x 140 μm^2 aperture size, containing 50 x 50 meta-atoms in total. The phase profile for each meta-atom under both x and y-polarized incidence was individually calculated and later used as phase inputs for the generative network, as shown in Fig. 6c. All amplitude profiles are designated to be uniform to maximize the focusing efficiency. Only a quarter of the metasurface lens was designed (Fig. 6d), with the whole pattern being generated from symmetry by mirroring this quarter along the x and y axes. Electromagnetic responses for each meta-atom are simulated and presented in Fig. 6e and 6f, respectively. Full wave simulation for the whole lens is carried out. The electric fields in the y-z plane under two different polarization directions are plotted in Fig. 6g, where a diffraction-limited focal spot is observed for each case. The electric fields along the optical axis are also simulated and plotted in Fig. 6g for the purpose of comparison, where two distinct E-field peaks can be clearly observed at 60 μm and 80 μm, respectively.

Most metadevices provide functionalities for a specified linear or circular-polarized incidence only [3, 9-12]. A widely-adopted route to overcome this limitation is to realize meta-devices using polarization-independent meta-atoms which have centrosymmetric shapes [29, 34, 35]. Alternatively, we utilized our dual-polarization meta-atom generative network to design a polarization-insensitive transmissive focal lens by equalizing the focal length of the focal-reconfigurable lens to be 80 μm (Fig. 7). One way to achieve this goal is enforcing that the phase shifts for x and y polarization are identical which yielded mostly structures that feature 4-fold rotational symmetry (in accordance with their polarization-insensitive nature). However, since some of these phase and amplitude combinations are physically not achievable, the overall efficiency of the lens realized in this way is relatively low, as shown by the dark blue areas in Fig. 7b. Some of the phase requirements are also not fulfilled (e.g. $-\pi$ phase shift are not achieved with the designs showing in Fig. 7a under x-polarized incidence).

The 4-fold rotational symmetry requirement can be relaxed by considering that the relative phase difference between two polarization states could be non-zero (in fact it only needs be maintained as a constant). Following this approach, with the help of dual-polarization meta-atom generative network, a 90 degree constant phase bias (difference) was added to the lens' phase mask under x-polarized plane wave incidence. The resulting design is shown in Fig. 7c. The updated meta-atom patterns are no longer 4-fold rotationally symmetric, indicating a new degree of design freedom. Meanwhile, the simulated amplitude profiles for the meta-atoms showing in Fig. 7d are significantly improved compared to the results shown in Fig. 7b. Following the same setup as in Fig. 6, the full wave simulated electric fields for the whole lens in Fig. 7c are plotted in Fig. 7e,f. The E-fields in the y-z plane under different polarization incidences share the same focal length of 80 μm with near-equal magnitude, validating the design concept.

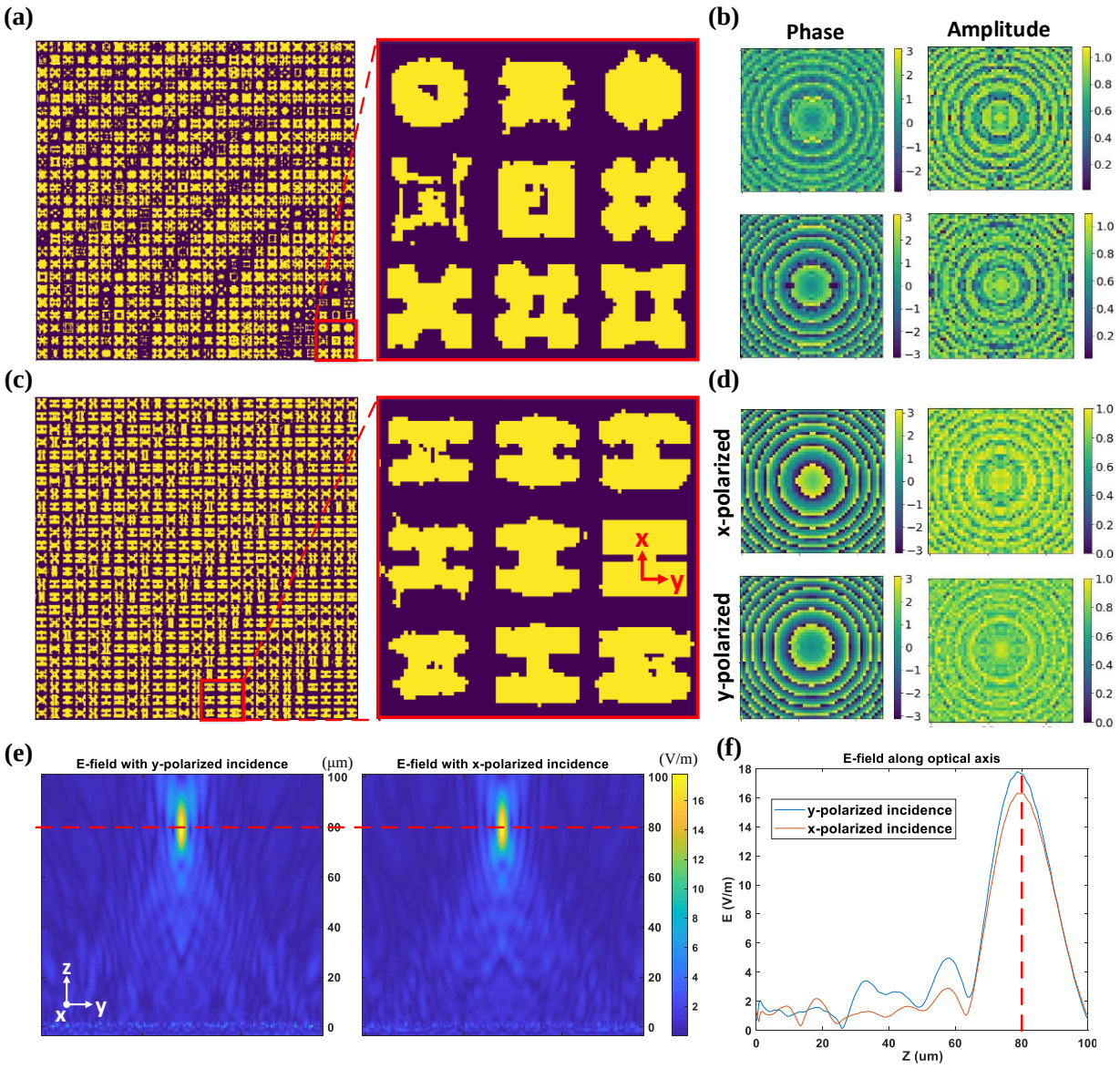

Figure 7. A polarization-independent focusing lens designed with the dual-polarization meta-atom generative network. (a) Metasurface pattern designed with the dual-polarization meta-atom generative network. Same absolute initial phase are used for two orthogonal directions. Part of the metasurface device circled in red lines was enlarged for a clear view. **(b)** Simulated phase and amplitude masks of the meta-atom patterns in (a) under x and y polarized incidence. **(c)** Another metasurface pattern designed with the dual-polarization meta-atom generative network with a 90 degree constant phase shift added to the targeted phase mask under x-polarized incidence and corresponding phase and amplitude masks under x and y polarized incidence are plotted in **(d)**. **(e)** Full wave simulated E-field in y-z plane under two orthogonal polarization incidences. Focal length remained 80 μm while polarization direction was switched. **(f)** Full-wave simulated E-field along optical axis under two orthogonal polarization directions.

As another demonstration of multifunctional metasurface devices, wideband transmissive metasurface modulators are designed using the proposed generative network. Wideband metasurface modulators [13, 14, 17, 22] normally require distinct transmission performances at different frequency points, which are non-intuitive and thus largely rely on trial-and-error

approaches. Meanwhile, design complexity of the proposed deep learning-enabled metasurface/metamaterial inverse design network is not affected by the size or the relevance of the inputs, which makes it a perfect solution to these devices. The network structure proposed in this paper was also slightly modified to build a meta-filter generative network. The condition vector x, is denoted as: $x = [T_{\omega 1}(y), T_{\omega 2}(y), \cdots, T_{\omega N}(y)]$, where N represents the number of the frequency points used to sample the whole spectrum. We consider a relatively wideband spectrum covering from 30 THz to 60 THz, which is 5-10 μm in wavelength. A total number of 31 frequency points, with a spacing of 1THz, were chosen to sample the spectrum. After the training had been fully converged, several sample patterns were created with different target transmission conditions using the trained generative model, with the results plotted in Fig. 8, along with the corresponding electromagnetic responses obtained through full wave simulations.

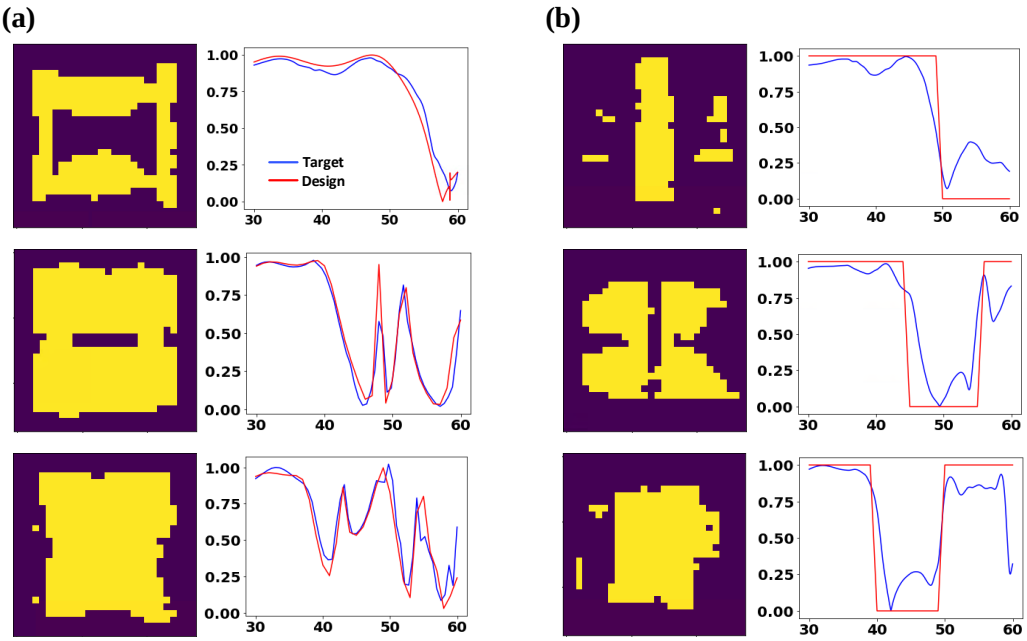

Figure 8. A wideband transmissive metasurface modulator designed with the meta-filter generative network for (a) Targeted spectral responses are from training datasets and **(b)** targeted spectral response are user-defined. Blue curves represent targeted spectrum while red curves represent spectral responses of generated designs.

From Fig. 8, we can conclude that the transmission spectra of network-generated meta-atoms agree well with the targeted spectral responses, under the cases where targeted responses are from the training datasets (Fig. 8a) and user-defined (Fig. 8b). This indicates the extraordinary "extrapolating" capability of the proposed network, which isn't necessarily limited by the training data distribution P_{data}. Moreover, it is worth to point out that all the data in the training datasets are symmetrical along the x and y axes, whereas the patterns in Fig. 8 (b) with good performances are asymmetrical, which further indicates that the proposed geometrical interpolation method for the generative network can explore the real distribution P_{real} from P_{data}.

Conclusion. In this paper, a multifunctional meta-atom design network based on the conditional WGAN architecture was proposed and demonstrated. For the first time, a novel Gradient Penalty method, along with a customized split complex coefficient data feeding approach was proposed and adopted to stabilize the training. With the fully trained multifunctional meta-atom generative model, a hologram operating at 50THz, a dual-polarized focal-reconfigurable lens, a polarization-independent lens and a broadband transmissive modulator were designed and verified by full-wave simulations. Good agreement has been achieved between numerical results and theory & calculations. We envision that this deep-learning-based design approach can be readily applied to not only other multifunctional metasurfaces/meta-atoms, but various types of electromagnetic devices, such as microwave components, antennas and integrated optical circuit designs. It can be further extended to address other complex problems in science and engineering.

Reference

1. H. C. Hulst, H. C. van de Hulst, *Light scattering by small particles*. (Courier Corporation, 1981).
2. J. D. Jackson, *Classical electrodynamics*. (John Wiley & Sons, 2007).
3. Q. Wang *et al.*, Broadband metasurface holograms: toward complete phase and amplitude engineering. *Scientific reports* **6**, 32867 (2016).
4. A. Arbabi, Y. Horie, M. Bagheri, A. Faraon, Dielectric metasurfaces for complete control of phase and polarization with subwavelength spatial resolution and high transmission. *Nature nanotechnology* **10**, 937 (2015).
5. N. Yu, F. Capasso, Flat optics with designer metasurfaces. *Nature materials* **13**, 139 (2014).
6. S. Jahani, Z. Jacob, All-dielectric metamaterials. *Nature nanotechnology* **11**, 23 (2016).
7. M. Khorasaninejad *et al.*, Achromatic metalens over 60 nm bandwidth in the visible and metalens with reverse chromatic dispersion. *Nano letters* **17**, 1819-1824 (2017).
8. S. M. Kamali, A. Arbabi, E. Arbabi, Y. Horie, A. Faraon, Decoupling optical function and geometrical form using conformal flexible dielectric metasurfaces. *Nature communications* **7**, 11618 (2016).
9. X. Wang *et al.*, Simultaneous realization of anomalous reflection and transmission at two frequencies using bi-functional metasurfaces. *Scientific reports* **8**, 1876 (2018).
10. J. Ding, S. An, B. Zheng, H. Zhang, Multiwavelength Metasurfaces Based on Single-Layer Dual-Wavelength Meta-Atoms: Toward Complete Phase and Amplitude Modulations at Two Wavelengths. *Advanced Optical Materials* **5**, 1700079 (2017).
11. T. Wang *et al.*, Dual-Band High Efficiency Terahertz Meta-Devices Based on Reflective Geometric Metasurfaces. *IEEE Access* **7**, 58131-58138 (2019).
12. L. Liu *et al.*, Broadband metasurfaces with simultaneous control of phase and amplitude. *Advanced materials* **26**, 5031-5036 (2014).
13. D. Liu, Y. Tan, E. Khoram, Z. Yu, Training deep neural networks for the inverse design of nanophotonic structures. *ACS Photonics* **5**, 1365-1369 (2018).
14. Z. Liu, D. Zhu, S. P. Rodrigues, K.-T. Lee, W. Cai, Generative model for the inverse design of metasurfaces. *Nano letters* **18**, 6570-6576 (2018).
15. W. Ma, F. Cheng, Y. Liu, Deep-learning-enabled on-demand design of chiral metamaterials. *ACS nano* **12**, 6326-6334 (2018).
16. I. Malkiel *et al.*, Plasmonic nanostructure design and characterization via Deep Learning. *Light: Science & Applications* **7**, 60 (2018).
17. J. Peurifoy *et al.*, Nanophotonic particle simulation and inverse design using artificial neural networks. *Science advances* **4**, eaar4206 (2018).
18. S. An *et al.*, A Novel Modeling Approach for All-Dielectric Metasurfaces Using Deep Neural Networks. *arXiv preprint arXiv:1906.03387*, (2019).
19. I. Goodfellow *et al.*, in *Advances in neural information processing systems*. (2014), pp. 2672-2680.
20. M. Mirza, S. Osindero, Conditional generative adversarial nets. *arXiv preprint arXiv:1411.1784*, (2014).
21. J. Jiang *et al.*, Data-driven metasurface discovery. *arXiv preprint arXiv:1811.12436*, (2018).
22. J. Jiang, J. A. Fan, Dataless training of generative models for the inverse design of metasurfaces. *arXiv preprint arXiv:1906.07843*, (2019).
23. J. Jiang, J. A. Fan, Global optimization of dielectric metasurfaces using a physics-driven neural network. *arXiv preprint arXiv:1906.04157*, (2019).
24. Z. Liu *et al.*, Compounding meta-atoms into meta-molecules with hybrid artificial intelligence techniques. *arXiv preprint arXiv:1907.03366*, (2019).
25. D. Sell, J. Yang, S. Doshay, J. A. Fan, Periodic Dielectric Metasurfaces with High-Efficiency, Multiwavelength Functionalities. *Advanced Optical Materials* **5**, 1700645 (2017).

26. H. Cheng *et al.*, Integrating polarization conversion and nearly perfect absorption with multifunctional metasurfaces. *Applied Physics Letters* **110**, 171903 (2017).
27. F. Callewaert, V. Velev, P. Kumar, A. Sahakian, K. Aydin, Inverse-designed broadband all-dielectric electromagnetic metadevices. *Scientific reports* **8**, 1358 (2018).
28. R. C. Devlin, M. Khorasaninejad, W. T. Chen, J. Oh, F. Capasso, Broadband high-efficiency dielectric metasurfaces for the visible spectrum. *Proceedings of the National Academy of Sciences* **113**, 10473-10478 (2016).
29. E. Arbabi, A. Arbabi, S. M. Kamali, Y. Horie, A. Faraon, Multiwavelength polarization-insensitive lenses based on dielectric metasurfaces with meta-molecules. *Optica* **3**, 628-633 (2016).
30. M. Arjovsky, S. Chintala, L. Bottou, in *International conference on machine learning*. (2017), pp. 214-223.
31. I. Gulrajani, F. Ahmed, M. Arjovsky, V. Dumoulin, A. C. Courville, in *Advances in neural information processing systems*. (2017), pp. 5767-5777.
32. K. He, X. Zhang, S. Ren, J. Sun, in *Proceedings of the IEEE international conference on computer vision*. (2015), pp. 1026-1034.
33. S. Ioffe, C. Szegedy, Batch normalization: Accelerating deep network training by reducing internal covariate shift. *arXiv preprint arXiv:1502.03167*, (2015).
34. M. Khorasaninejad *et al.*, Polarization-insensitive metalenses at visible wavelengths. *Nano Letters* **16**, 7229-7234 (2016).
35. K. E. Chong *et al.*, Polarization-independent silicon metadevices for efficient optical wavefront control. *Nano letters* **15**, 5369-5374 (2015).

Acknowledgements

This work was funded under Defense Advanced Research Projects Agency Defense Sciences Office (DSO) Program: EXTREME Optics and Imaging (EXTREME) under Agreement No. HR00111720029.